

RELATION BETWEEN SOURCE AND TEMPERATURE FLUCTUATIONS IN PHOTOIONIZED NEBULAE

Luc Binette ¹, Pierre Ferruit ², Wolfgang Steffen ¹ and Alejandro Raga ³

Submitted to RevMexAA 16th December 2018

RESUMEN

La magnitud de las fluctuaciones de temperatura (t^2) que se necesitan para explicar las incoherencias observadas entre las metalicidades inferidas por las líneas de recombinación o por las líneas prohibidas, no pueden alcanzarse con modelos al equilibrio y estacionarios en el tiempo. Por otra parte, si la fuente ionizante fuera variable, las fluctuaciones de temperaturas t^2 serían mucho mayores. Investigamos la respuesta temporal de la estructura en ionización y temperatura de una nebulosa fotoionizada por una fuente variable periódica. Estudiamos como el valor medio asintótico, $\langle t^2 \rangle$, se comporta en función del período y amplitud de las variaciones de la fuente. Encontramos que las fluctuaciones de temperatura se producen solamente en la parte externa de la nebulosa, cerca del frente de ionización, dentro de un espesor geométrico correspondiente al 8-20% del tamaño de la capa ionizada. Concluimos que la amplitud de variación de la estrella excitadora que se requiere para conseguir un $\langle t^2 \rangle = 0.025$ (como en la nebulosa de Orion) es excesivamente grande. La variabilidad de la fuente ionizante no es por lo tanto un mecanismo viable para explicar los valores observados de t^2 . Llegamos a conclusiones similares cuando estudiamos la variabilidad temporal que resulta de sombras intermitentes detrás de condensaciones de gas opacas. Encontramos que nebulosas fotoionizadas son en promedio menos masivas pero algo más calientes en el caso de fuentes variables cíclicas.

ABSTRACT

The magnitude of the temperature fluctuations (t^2) required to explain the observed inconsistencies between metallicities inferred from recombination lines and from forbidden lines cannot be attained by steady-state equilibrium photoionization models. If on the other hand the nebular ionizing source was variable, the temperature fluctuations t^2 would be significantly larger. We investigate the time-dependent response of the nebular ionization and temperature structure when photoionized by a periodically varying source. We study how the asymptotic mean value, $\langle t^2 \rangle$, behaves as a function of the period or amplitude of the source variability. We find that the temperature fluctuations occur only in the outer section of the nebula, close to the ionization front, within a zone corresponding to 8–20% of the ionized layer's thickness. We conclude that the amplitude of the exciting star variations required to achieve a $\langle t^2 \rangle = 0.025$ (as in the Orion nebula) is unacceptably large. Source variability is therefore not a viable mechanism to explain the observed values of t^2 . We reach a similar conclusion from studies of the temporal variability resulting from intermittent shadows behind opaque condensations. We find that photoionized nebulae are on average less massive but somewhat hotter in the case of cyclicly variable ionizing sources.

Key Words: ISM: HII REGIONS — LINE: FORMATION — RADIATIVE TRANSFER

1. INTRODUCTION

The presence of temperature fluctuations in photoionized nebulae has been a matter of debate since the pioneering work of Peimbert (1967). Observational evidence has since accumulated in favor of his analysis of the problematics of nebular temperatures. For instance, the temperatures of HII regions and planetary nebulae are observed to be significantly

lower when derived using recombination lines rather than from forbidden line ratios (see review by Peimbert et al. 1995).

The work of Kingdon & Ferland (1995) and Pérez (1997) has shown that the amplitude of the fluctuations in hydrostatic photoionization calculations are much smaller than required to explain the observed differences between forbidden and recombination lines temperatures. Possible causes for the fluctuations include metallicity inhomogeneities (Torres-Peimbert et al. 1990; Kingdon & Ferland 1998; Liu et al. 2000), photoionization by small dust grains

¹Instituto de Astronomía, Universidad Nacional Autónoma de México

²CRAL – Observatoire de Lyon

³Instituto de Ciencias Nucleares, Universidad Nacional Autónoma de México

(Stasińska & Szczerba 2001), and shock heating due to stellar wind or even supernovae in the case of giant H II regions (Luridiana et al. 1999). The inclusion of temperature fluctuations in a theoretical framework has so far been tentative (Luridiana, Cerviño & Binette 2001; Binette & Luridiana 2000; Binette, Luridiana & Henney 2001) given our lack of knowledge about their possible cause.

In this Paper, we investigate how temporal variability in ionization structure due to an intrinsically variable ionizing source or to intermittent shadows behind opaque condensations can affect the temperature structure and induce substantial temperature fluctuations. We also address the question whether a variable ionizing continuum with a fixed duty cycle would lead to a nebula that is on average warmer and less massive.

2. CALCULATIONS

2.1. Intrinsic variability of the ionizing source

Resolution of the ionizing radiation transfer in the case of a variable source implies a sufficiently high temporal resolution in order to follow the progression of ionizing photon fronts across the nebula. The atomic timescales on the other hand are much longer, and a lot of computation time is spent in the actual transfer while not much is occurring in terms of changes in ionization or temperature. For this reason, in the building of the new code YGUANA we simplified the atomic physics in order to derive the desired results within reasonable computation efforts. Our goal was to give precedence to a rigorous treatment of the transfer, and not to detailed atomic physics. The Courant condition, for instance, was rigorously satisfied in all the calculations (Eq. 20 in Appendix B.2.1).

One of the simplifications introduced in YGUANA is that only Hydrogen is considered in the integration of the nebular opacity, which is a valid approximation for H II regions. Furthermore, we consider a monochromatic transfer with all ionizing photons having the same energy. This simplification implies that the hardening of the ionizing radiation with depth is not considered. The expected shallow radial temperature gradient will therefore be absent from our calculations. This is a minor shortcoming of YGUANA, since the level of temperature fluctuations caused by non-equilibrium ionization largely exceed that produced by the temperature gradient alone (c.f. §2.4). In effect, non-equilibrium photoionization within the IF, which we compute accurately, far exceeds the larger increased due to continuum hardening at large depths. The various effects introduced by UV source variability on a photoionized

nebula will all be accurately tracked and made obvious by comparing our time-dependent nebula to either the time-averaged nebula or to the steady-state constant-UV reference nebula.

The cooling by metals was approximated in YGUANA by a fit we made to the cooling function using MAPPINGS IC (Ferland et al. 1997) [c.f. Appendix A]. Collisional excitation and ionization of H I (and their effect on cooling) are calculated explicitly, since they can become important within the ionization front (IF). The time-dependent ionization balance of H, the photoheating coefficients, and the equation of state are described in Appendix A while the practical implementation of the time-dependent transfer equations are presented in Appendix B. Our main goal is to study the effect on the temperature fluctuations measured *à la* Peimbert as a result of having a variable ionizing source. Our model assumes an hydrostatic distribution of gas.

2.2. Mean temperature \bar{T}_0 , t^2 and \bar{U}

Following Peimbert (1967), we define the mean nebular temperature, \bar{T}_0 , as follows

$$\bar{T}_0(\text{H}^+) = \frac{\int_V n_e n_{\text{H}^+} T dV}{\int_V n_e n_{\text{H}^+} dV}, \quad (1)$$

where n_e is the electron density, n_{H^+} the H II density, T the electron temperature and V the volume over which the integration is carried out. The rms amplitude t of the temperature fluctuations is given by

$$t^2(\text{H}^+) = \frac{\int_V n_e n_{\text{H}^+} (T - \bar{T}_0)^2 dV}{\bar{T}_0^2 \int_V n_e n_{\text{H}^+} dV}. \quad (2)$$

We have replaced n_{H^+} by n_e in the above expressions, since we do not consider explicitly He in the calculations. n will denote the total H density.

We cannot compute t^2 for other ions, since we consider in detail only the ionization of H. We will drop the label H^+ in the following discussion unless required by the context.

In the case of a variable source, both global quantities t^2 and T_0 vary with time. The above expressions define therefore instantaneous values for a particular time in the source temporal evolution. Even if the transfer of information concerning n_{H^+} , n_{H^0} or T from any position inside the nebula has a finite speed, we do not find necessary to consider this effect explicitly, since we are not considering any particular external observer. Furthermore, our derivation of various characteristic quantities (labeled “asymptotic”) will be done by integrating over a few full

periods of the source variability. This has the effect of washing out any phase differences introduced by placing a real observer at any particular external location.

Let us define further useful quantities to be used later. One is the varying ionizing source photon luminosity, Q_H . Time-averaged quantities will carry brackets $\langle \rangle$ such as in $\langle Q_H \rangle$, the time-averaged photon luminosity. Since we adopt a spherical geometry and consider the source point-like, the global ionization parameter is defined as

$$\bar{U} = \frac{\int_V \epsilon^2 n_e^2 \frac{\varphi}{c n} dV}{\int_V \epsilon^2 n_e^2 dV} = \frac{\int_{r_0}^{R_s} \epsilon^2 n_e^2 \frac{\langle Q_H \rangle}{4\pi r^2 c n} 4\pi r^2 dr}{\int_{r_0}^{R_s} \epsilon^2 n_e^2 4\pi r^2 dr} \quad (3)$$

where φ is the local ionizing flux (disregarding opacity), τ_H the opacity due to H photoionization, R_s the outer nebular radius, r the distance from the central source, r_0 the radius of the inner cavity devoid of gas, ϵ the volume filling factor, and c the speed of light. (This definition contemplates the possibility that ϵ and the total density n may vary with radius.)

2.3. Results for periodical sources (Model A)

Our main goal is to derive the characteristic $\langle t^2 \rangle$ of a nebula submitted to a variable ionizing source. The general problem is excessively vast since there are numerous scenarios about possible variability behaviors. The perspective taken in this Paper is that of a Fourier analysis in which we restrict ourselves to the exploration of periodical sources and analyze the nebular response as a function of the frequency and amplitude of the source variability. In concrete terms, we have narrowed the problem to deriving the *asymptotic* $\langle t^2 \rangle$ for a source varying at a predetermined frequency. We define the asymptotic $\langle t^2 \rangle$ as the averaged value over at least three full periods of the source. This has the advantage of avoiding a definition that depended on the initial conditions or on a particular ill-defined moment in the source history. Typically, calculations will extend to only five periods since we found that asymptotic values in most cases do not change by adding more cycles.

A varying source generate two types of response in the nebular structure: a progressing IF when the source increases in intensity and a recombination front (RF) when the source decreases. These two phases are not symmetric. For instance, an IF has a finite velocity given by $V_{IF} \simeq \varphi/n_{H^0} < c$, where φ is the ionizing photon flux. Let us define y as the neutral fraction of H. The ionization fraction $(1 - y)$ within the IF can increase at a rate, which is much shorter than the recombination timescale. An RF

on the other hand propagates at the speed c , since a RF is initiated following propagation of the signal that the source is decreasing (although the neutral H fraction y within the front will increase only on timescales given by recombination).

To illustrate these two phases, using YGUANA we will study in detail the case of source varying like a square-wave⁴ with a period Π equal to the recombination timescale $\tau_{rec} = (\alpha_B n_e)^{-1}$, where α_B is the recombination coefficient rate to excited states of H. The amplitude of the variability is $\pm 20\%$ ($A = 0.20$) and the duty cycle is $\Delta = 0.5$. The advantage of the square-wave is that it will more clearly reveal the changes caused by either type of fronts on certain nebular quantities. We will assume an ionizing photon luminosity of $\langle Q_H \rangle = 10^{51} \text{s}^{-1}$ and a nebula of constant density $n = 200 \text{cm}^{-3}$ with a volume filling factor of $\epsilon = 0.01$ and an inner cavity r_0 surrounding the source of 30% of the estimated Strömgren radius, that is, of size $r_0 = 4.0 \times 10^{19} \text{cm}$. The initial physical conditions of the gas were given by the usual condition of steady-state thermal and ionization equilibrium, throughout the whole nebula, for a source luminosity $\langle Q_H \rangle$. The equilibrium temperature within the nebula turns out to be $T_{eq} = 5260 \text{K}$ and the recombination and cooling timescales within the fully ionized part of the nebula are $\tau_{rec} = 1.1 \times 10^{10} \text{s}$ and $\tau_{cool} = 1.6 \times 10^9 \text{s}$, respectively (the cooling timescale is 7 times shorter than τ_{rec}). The ionization parameter (Equation 3) of the initial equilibrium model is $\bar{U} = 0.0022$. This set of parameters defines our Model A.

The results of the time-dependent calculations as a function of time τ for the first five periods are shown in Fig. 1. The dotted line in Panel *a* illustrates the behavior of the ionizing flux relative to the mean value (to be read on the upper right y -axis of Panel *a*). In all the panels, the continuous line corresponds to the behavior of the instantaneous values integrated over the whole nebula while the long-dashed line represents the cumulative running mean, which was calculated at the onset of the third variability cycle. We define asymptotic values as the last value of the running mean (after the 5th cycle is completed). The impact on the nebula of the progression of the IF or the recession of the RF are clearly visible in Panel *d*, which is a plot of the mass of ionized gas normalized to the initial equilibrium value. Notice that the total ionized mass of the nebula somewhat shrinks with time. Panel *c* shows the

⁴We will use primes to denote models that assume a *sine-wave* (rather than *square-wave*) variability, e.g. Model A'' in §2.7.

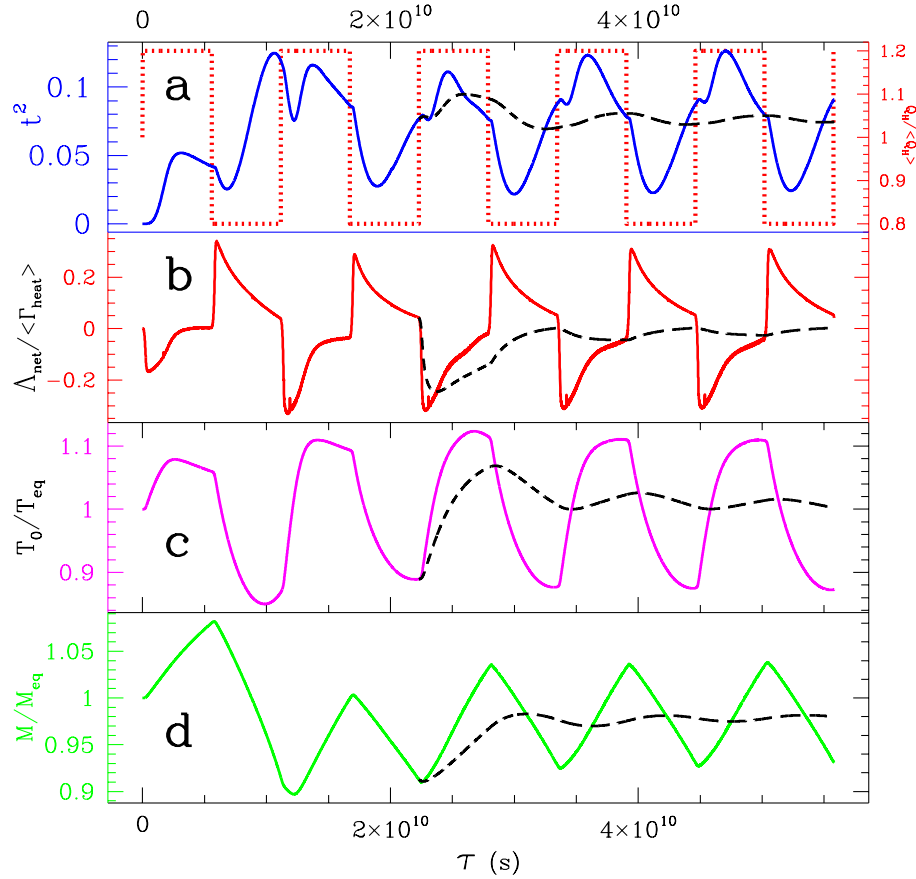


Fig. 1. All solid lines: behavior of nebular volume weighted quantities as a function of time τ for Model A. Panel *a*: t^2 , Panel *b*: net cooling relative to the mean heating energy radiated by the source $\Lambda_{net}/\langle\Gamma_{heat}\rangle$ [with $\langle\Gamma_{heat}\rangle = h(\bar{\nu} - \nu_0) \langle Q_H \rangle$], Panel *c*: the mean electron temperature \bar{T}_0/T_{eq} , and Panel *d*: the mass of ionized gas M/M_{eq} . In each panel, the long-dashed line across the last three cycles represents the running mean of the plotted quantity. The asymptotic values referred to in the text (e.g. $\langle\bar{T}_0\rangle$, $\langle t^2 \rangle$) correspond to the rightmost value along the long-dashed line. The *square-wave* dotted-line in Panel *a* is the normalized photon luminosity of the ionizing source as a function of time, $Q_H(\tau)/\langle Q_H \rangle$ (to be read on the upper right y -axis). The variability is characterized by an amplitude $A = 0.2$, a period $\Pi = \tau_{rec}$ and a duty cycle $\Delta = 0.5$.

behavior of the average nebular temperature with time, $\bar{T}_0(\tau)$, normalized again to the initial equilibrium value T_{eq} . Panel *b* shows the behavior of the net integrated cooling rate of the nebula normalized to the total heating available due to absorption of all ionizing photons (this ratio cannot exceed the interval ± 1). With steady-state equilibrium, the net cooling is zero. Panel *b* reveals how the nebula as a whole heats up during the IF phase while it cools down during the RF phase. Finally, Panel *a* illustrates the behavior of t^2 as a function of time. Its (asymptotic) average value is $\langle t^2 \rangle = 0.074$.

2.4. Missing the temperature gradient

Not considering the hardening of the UV radiation with depth results in an isothermal nebula lacking the usual outward gradient in T_{eq} . This has the advantage that t^2 computed with YGUANA is determined by source variability alone. The effect of missing the shallow T_{eq} gradient is negligible in most cases. In effect, using MAPPINGS IC, we find that the constant-UV steady-state Model A is characterized⁵ by a $t^2_{steady} = 0.0026$, which is generally very small in comparison with the values derived for the variable sources studied below. The true t^2 , which would include UV hardening, cannot be far off from the following estimate $t^2_{true} \approx t^2_{steady} + \langle t^2 \rangle$, where $\langle t^2 \rangle$ corresponds to the time-averaged fluctuation amplitudes computed using YGUANA. We recall that $\langle t^2 \rangle = 0.074$ for Model A with $A = 0.2$.

2.5. The internal nebular structure

The changes taking place within the spherical nebula of Model A occur mostly within the external parts, that is within the outer 25%, which corresponds nonetheless to half the photoionized volume. This becomes apparent in Fig. 2 where the H neutral fraction, y , and the local temperature are plotted as a function of nebular geometrical depth $r - r_0$. The long-dashed line represents the initial equilibrium model. The lack of any slope in the equilibrium temperature curve (dashed-line) in Panel *b* is the result of not considering the hardening of ionization radiation with depth (the transfer in YGUANA is monochromatic, but see §2.4). The 10 solid lines correspond to the ionization and thermal structure at equally spaced time intervals during the last (fifth) variability cycle (see last cycle in Fig. 1a). The IF phase corresponds to the 5 curves below the dashed-line in Panel *a* while the other 5 curves correspond

to the RF phase. During the RF phase, the neutral fraction lies above the dashed-line equilibrium curve (except near the transition to neutral gas, where $y \sim 1$). The progression of the IF is characterized, on the other hand, by a sharp temperature pulse above the equilibrium value, which is spatially resolved in YGUANA (see Fig. 2b). This IF is sufficiently hot to cause a rise in the mean temperature (averaged over the whole nebula) as seen in Fig. 1c. Because the selected source period is rather long, being equal to τ_{rec} , most of the inner nebula has time to adjust its ionization while the source varies. This is shown by the coincidence of most curves for geometrical depths $r - r_0 < 6 \times 10^{19}$ cm, as they lie (and superimpose) either below or above the equilibrium y dashed-line model in Fig. 2a.

Interestingly, the temporal changes in the neutral fraction y with time for depths $r - r_0 \leq 5 \times 10^{19}$ cm does not cause any appreciable changes in the gas temperature (see Panel *b*). The reason is that during the IF or RF phase, the neutral fraction y in that zone evolves quickly toward the appropriate equilibrium (but small) value y_{eq} over a timescale of order $\sim 0.5y_{eq}\tau_{rec}$, which is much shorter than τ_{rec} (because $y_{eq} < 0.01$ in that zone). Hence, non-equilibrium heating is too short-lived in that inner zone for the temperature to change appreciably.

2.6. Varying the ionization parameter \bar{U} (Model B)

The work of Campbell (1988) indicates that the ionization parameter⁶ in H II galaxies range from 0.0014 to 0.025. Hence Model A ($\bar{U} = 0.0022$) is probably representative of nebulae⁷ at the low \bar{U} end. We have explored the behavior of $\langle t^2 \rangle$ when the ionization parameter is varied. This was done by setting the filling factor ϵ to unity and computing models which were characterized by different cavity sizes. By varying r_0 in the interval $2.5 \times 10^{19} \leq r_0 \leq 1.5 \times 10^{20}$ cm, we explored the following range 0.018–0.0006 in \bar{U} (we assumed a source variability of $A = 0.05$ with the other parameters such as n , Δ , Π , $\langle Q_H \rangle$ the same as in Model A). What we found was that $\langle t^2 \rangle$ increased approximately as $\sqrt{\bar{U}}$ within the above range.

⁶The definition of \bar{U} of Campbell (1988) is slightly different, which causes the values quoted by her to be 50% higher than those one would derive using eq. (3)

⁷Models of different densities, filling factors and source luminosities but whose product of $n \times \epsilon^2 \times \langle Q_H \rangle$ is the same as well as the ratio r_0/R_S^0 , where R_S^0 is the Strömgren radius in the cavity-less case ($R_S^0 = [3 \langle Q_H \rangle / 4\pi n^2 \epsilon \bar{\alpha}_B]^{1/3}$), are homologous and can therefore be expected to yield the same $\langle t^2 \rangle$ values under similar variability conditions [i.e. variations of similar amplitude A and period Π (in τ_{rec} units)].

⁵The values of $t^2(O^{+2})$ computed by MAPPINGS IC in the constant-UV case for Models A and B are 0.0021 and 0.0047, respectively.

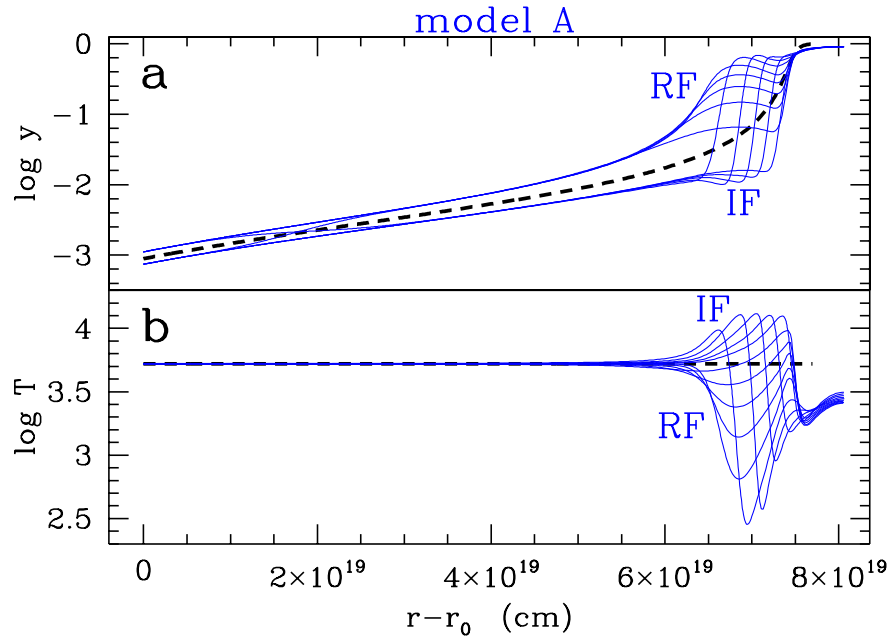


Fig. 2. Internal structure of the nebula as a function of geometrical depth for Model A (c.f. § 2.3) assuming a *square-wave* variability of amplitude $A = 0.20$. Panel *a*: the neutral fraction y of H, Panel *b*: the local temperature T . The long-dashed line represents the initial equilibrium model. The 10 solid lines correspond to the ionization and thermal structure at equally spaced time intervals during the last full cycle shown in Fig. 1a.

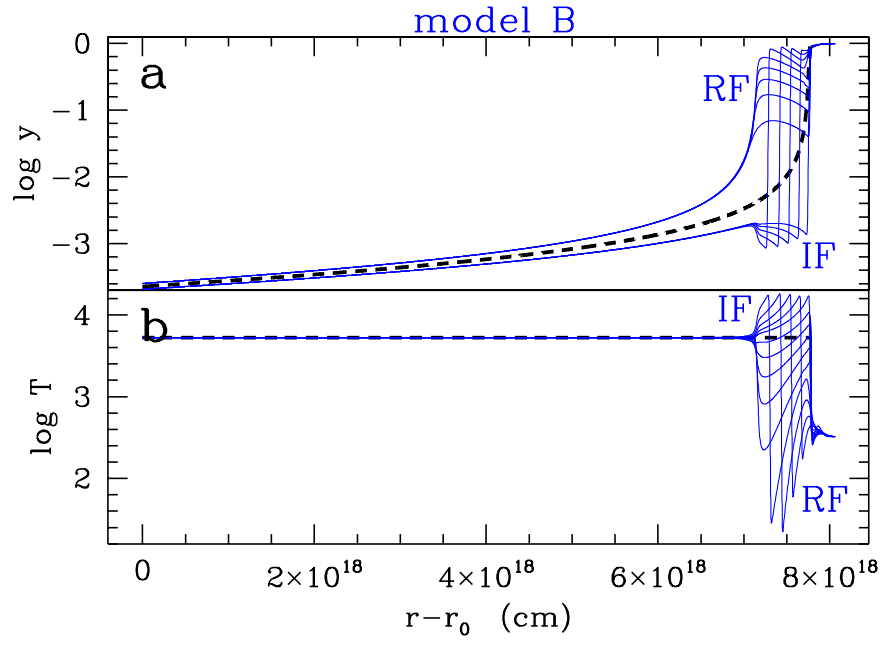


Fig. 3. Internal structure of the nebula as a function of geometrical depth for Model B (c.f. § 2.6) assuming a *square-wave* variability of amplitude $A = 0.10$. Panel *a*: the neutral fraction y of H, Panel *b*: the local temperature T . The long-dashed line represents the initial equilibrium model. The 10 solid lines correspond to the ionization and thermal structure at equally spaced time intervals during the last full cycle.

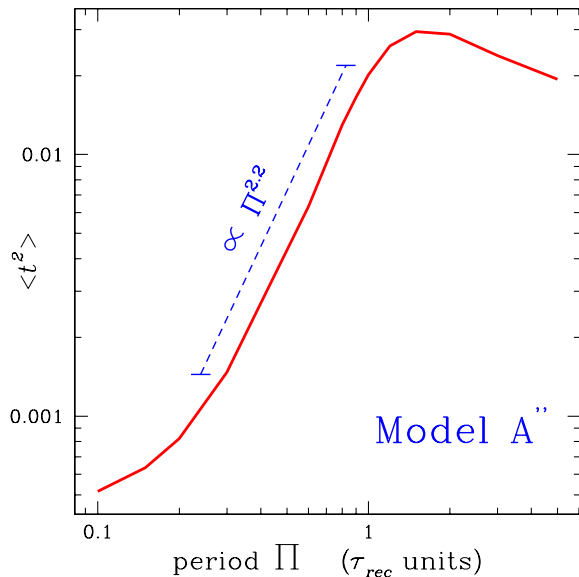


Fig. 4. Behavior of the asymptotic $\langle t^2 \rangle$ as a function of the period Π for a *sine-wave* variability of amplitude $A = 0.1$ (Model A''). In the interval $0.2 \leq \Pi \leq 1$, $\langle t^2 \rangle$ increases steeply as $\Pi^{2.2}$.

We also studied the properties of nebulae that reflect more closely the geometrical particularities of the Orion nebulae, that is a model consisting of a thin sheet of ionized gas at a much higher ionization parameter. For instance, the Orion model of Baldwin et al. (1991) is characterized by a slab geometry at an ionization parameter of 0.03. We reproduced similar characteristics by using $r_0 = 2 \times 10^{19}$ cm and by setting the filling factor ϵ to unity. With $\langle Q_H \rangle = 10^{51} \text{ s}^{-1}$ and a density $n = 200 \text{ cm}^{-3}$, the thickness of the ionized layer turns out to be 7.1×10^{18} cm, that is 26% only of the final Strömgren radius. The ionization parameter (Equation 3) of the initial equilibrium model is $\bar{U} = 0.024$. This set of parameters defines our Model B.

In Fig. 3, we show the internal temperature and ionization structure of Model B for a variability amplitude of $A = 0.10$. This model is characterized⁸ by an asymptotic $\langle t^2 \rangle$ of 0.053. Overall, Models B and A share many similarities. For instance, the bulk of the variability in T or y occurs near the outer IF.

2.7. Sensitivity to the period Π

Using a square wave variability type, we have illustrated the principal effects taking place within a nebula submitted to a periodical ionizing source.

⁸Using MAPPINGS 1c, we find that the constant-UV steady-state Model B is characterized by $t_{steady}^2 = 0.01$ (see §2.4).

Two very important parameters affect the nebular response and the behavior of $\langle t^2 \rangle$: the variability period Π and the amplitude of the variations A . We will analyze in turns the role played by each, adopting the same parameters as in Model A but with a sine-wave variability function $(1 + A \sin 2\pi\tau/\Pi)$ rather than a square wave. We will refer to this modified model as Model A''. We have verified that sine-wave models⁹ with amplitude $1.4A$ closely match the $\langle t^2 \rangle$ from square-wave models with amplitude A . All periods will be expressed in units of the recombination time, which is the natural unit for the problem at hand.

Our results for Model A'', assuming an amplitude $A = 0.1$, show a very steep dependence with frequency as illustrated in Fig. 4. $\langle t^2 \rangle$ increases as $\propto \Pi^{2.2}$ up to $\Pi \simeq 1\tau_{rec}$ and then peaks near $1.6\tau_{rec}$. The short period regime becomes progressively ill-defined in our calculations. For instance, the asymptotic value of $\langle t^2 \rangle$ at $\Pi = 0.1$ requires up to 10 cycles, because the mean values keep evolving well beyond 5 cycles. If radiation hardening at large depths had been considered, $\langle t^2 \rangle$ would lie above the $t_{steady}^2 = 0.0026$ floor computed by MAPPINGS 1c (see §2.4). This would alter the curve in Fig. 4 only in the short period domain $\Pi \lesssim 0.4$.

The main conclusion is that a nebula acts as a low-pass filter with only the relatively ‘slow’ source variations causing important temperature fluctuations. Clearly, $\Pi \gtrsim 0.7$ is the frequency domain that favors the largest values of $\langle t^2 \rangle$.

2.8. Sensitivity to the amplitude A

Let us now vary the amplitude (up to the maximum, which is $A = 1$ in the case of a sine-wave), adopting the same sine-wave variability with $\Pi = 1$. The results are shown in Fig. 5a. The larger the amplitude, the higher $\langle t^2 \rangle$, as one would expect. In the case of Model A'', there is, first a regime of faster increase ($\propto A^{1.8}$) of $\langle t^2 \rangle$, followed by a slower increase regime ($\propto A^{1.1}$) above $A = 0.1$. For Model B'', the increase is $\propto A^{1.1}$ everywhere. The basic result from this plot is that an observed $t_{obs.}^2 \simeq 0.02$ would require a substantial variability amplitude of 0.09 and 0.05 from the source, for Models A'' and B'', respectively¹⁰, which is unacceptably high for O stars, as discussed in § 3.1.

⁹The values of $\langle t^2 \rangle$ for models A'' and B'' in the *sine-wave* case with $\Pi = 1\tau_{rec}$ and $A = 0.1$ are 0.023 and 0.039, respectively. For $A = 0.2$, it is 0.055 and 0.078, respectively.

¹⁰However, since in Model B'', $t_{steady}^2 = 0.01$ (§2.6), an amplitude of $A = 0.03$ would suffice in reproducing fluctuations at the level $\langle t^2 \rangle \simeq 0.01 = 0.02 - t_{steady}^2$ (see §2.4).

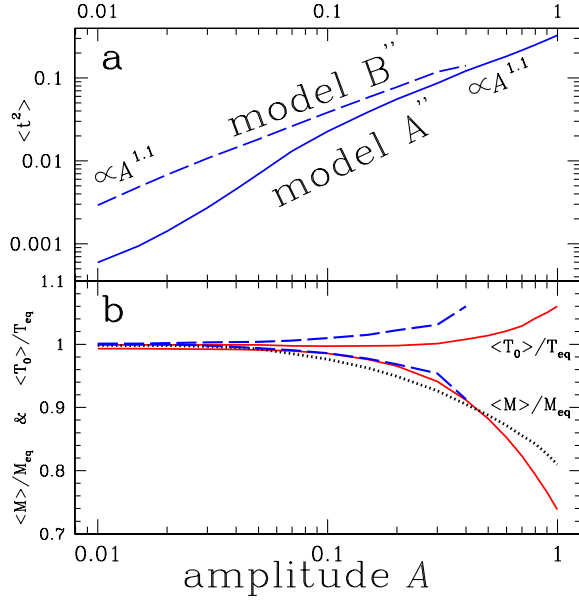


Fig. 5. Panel *a*: behavior of $\langle t^2 \rangle$ as a function of the amplitude of the *sine-wave* variations of Q_H . Panel *b*: behavior of $\langle \bar{T}_0 \rangle / T_{eq}$ (curves ≥ 1) and $\langle M \rangle / M_{eq}$ (curves ≤ 1) as a function of the amplitude of the *sine-wave* variations. Model A'' and B'' are represented using solid and dashed lines, respectively. The dotted line represents the equation $(1 + 0.7863\langle t^2 \rangle)^{-1.177} \langle \bar{T}_0 \rangle / T_{eq}$ (see § 2.8) using values from Model A''. Model B'' was not computed beyond $A = 0.4$.

An interesting phenomenon occurs with variable ionizing sources is that the mass of ionized gas shrinks as $\langle t^2 \rangle$ increases. For instance, for $A = 0.40$ in Model A'', the ionized mass is reduced to 91% of that of the initial steady-state equilibrium model. The reason is simple if we recall that temperature fluctuations (Peimbert 1967) in the case of a process like recombination, which is weighted towards lower temperatures ($\propto T^{-0.85}$), will lead to a higher efficiency of the recombination rate, hence to a lower mass of ionized gas in the nebula for a given mean ionizing flux. (The time-averaged luminosity of all recombination lines, however, remains the same.) Note finally the tendency of the mean temperature $\langle \bar{T}_0 \rangle$ to increase, at large amplitudes, slightly above the equilibrium value, as a result of the photoheating energy being absorbed more efficiently during the IF phase. The dotted line shows the approximate behavior expected for the ionized mass using the function $\langle M \rangle / M_{eq} \simeq (1 + 0.5\alpha(\alpha - 1)\langle t^2 \rangle)^{1/\alpha} \langle \bar{T}_0 \rangle / T_{eq}$ with $\alpha = -0.85$ (adapted from Equation 5 in Binette & Luridiana 2000). This expression becomes invalid above $\langle t^2 \rangle > 0.2$.

3. DISCUSSION

3.1. Intrinsic source variability

We have shown that variations of the ionizing luminosity can produce appreciable temperature fluctuations across the nebula. However, a careful analysis of our results leads us to believe that the proposed mechanism for generating fluctuations is not viable. For instance, to reproduce a $t_{obs.}^2 = 0.025$ as in the Orion nebula (Esteban et al. 1998) would require reproducing $\langle t^2 \rangle = 0.015 = 0.025 - t_{steady}^2$. This occurs with Model B'' (more appropriate to Orion) when $A = 0.04$, that is, it requires a variability of $\pm 4\%$ of the ionizing luminosity of the exciting star θ^1 C Ori (HD 37022), assuming $\Pi \simeq 1$. Such variability of Q_H would imply variations of order ± 250 K in the stellar atmosphere (derived from MAPPINGS IC using $T_* = 39500$). In the optical domain, the continuum variations would be a lot less, about $\pm 1\%$ in amplitude ($\Delta m_B = 0.02$ min-to-max). Furthermore, these estimates are based on a variability timescale very close to the recombination timescale, which is of order 20 years for Orion ($n_e \sim 5000 \text{ cm}^{-3}$), otherwise if it was shorter it would require variation amplitudes a lot larger (c.f. Fig. 4) in order to reproduce $t_{obs.}^2 = 0.025$ (i.e. $\langle t^2 \rangle = 0.015$). Although θ^1 C Ori has shown evidence of variability in the stellar He II absorption line (Conti 1972; Walborn 1981) and of a periodicity of 15 days in the H α equivalent width (Stahl et al. 1993), no photometric variations

of the continuum on timescales from days to years have been reported (van Genderen et al. 1989).

H II regions powered by Luminous Blue Variable (LBV) stars such as the Carina nebula are potential candidates for finding a cause and effect relation between t^2 and variability. One would expect t^2 to be significantly larger in nebulae excited by LBV stars. Unfortunately, we have no information at hand about t^2 in the Carina nebula for the purpose of comparison.

A general and compelling argument against source variability as the main cause of the fluctuations is that for metal lines like C III] $\lambda\lambda 1909$, [O III] $\lambda 5007$, the bulk of their luminosity occurs at a nebular depth such that $y < 10^{-1.7}$, the fluctuations in temperature (due to variability) are negligible in that inner zone of the nebula despite substantial changes in y , as shown in Fig. 2b. This means that $\langle t^2(\text{O}^{+2}) \rangle$ would be much smaller than $\langle t^2(\text{H}^+) \rangle$ calculated with model B'' and $A = 0.04$. (Even larger values of A would lead to insignificant values of $\langle t^2(\text{O}^{+2}) \rangle$.) In this particular model, it can be shown using MAPPINGS 1c that 90% of [O III] flux is emitted in the inner regions where no fluctuations occur due to variability, as illustrated in Fig. 3b. Therefore our models, based on the variability of Q_H , cannot realistically reproduce the large observed t_{obs}^2 , deduced from intermediate excitation emission lines.

3.2. Variable shadows from moving opaque condensations

There are other mechanisms than variable stars that can produce a transient variability in the propagating ionizing flux. For instance, the displacement of dense neutral condensations in planetary nebulae or H II regions (proplyds) can introduce temporal variations in the ionization structure. Within the shadow, behind these opaque condensations, the gas is either neutral or partly ionized by the diffused field from the surrounding nebula. If these condensations of lateral size D had a tangential velocity component V (distinct from the nebular gas), the tangential displacement of the shadow inside the nebula would produce effects similar to that of an ionizing source, which is switched off, then on again, generating in turns an RF and IF, respectively. The important timescales in this problem are τ_{rec} and τ_{cross} , the crossover timescale ($\tau_{cross} = D/V$) of the shadow over a distance given by the diameter of the opaque eclipsing condensation. We expect that the effect on the shadowed region would be strongest when τ_{cross} becomes comparable to τ_{rec} , since it would first in-

TABLE 1
FLUCTUATIONS FROM INTERMITTENTLY
SHADOWED IONIZED REGIONS

Π	Δ^a	$\Pi \times \Delta$	$\langle t^2 \rangle$
10	0.025	0.25	0.042
5	0.05	0.25	0.081
2.5	0.1	0.25	0.15
1.25	0.2	0.25	0.23
10	0.1	1.0	0.063
10	0.05	0.5	0.045
10	0.025	0.25	0.042
10	0.0125	0.125	0.021
10	0.00625	0.0625	0.013

^aFraction of cycle during which the ionizing flux is turned off.

duce a strong temperature drop and substantial recombination followed by the propagation of hot IF after the ‘‘eclipse’’ has ended. On the global scale of the nebula, these shadowed regions would cause temperature fluctuations similar to those calculated for a star that is briefly turned off. Whether the temperature fluctuations would be felt over the whole nebula would depend on how many such shadowed regions fill the nebular volume.

As an estimate of the t^2 expected in that case, we ran models in which the source was turned off during a time $(\Pi \times \Delta) \tau_{rec}$ where Π is the period of the off-on cycle in units of the recombination timescale and Δ is the fraction of the cycle during which the source is off. The idea behind using periodicity to approach this problem is that in this way we can crudely estimate the nebular fluctuations due to the shadows by associating Δ to the shadowed fraction, that is, to the effective covering factor of the source due to all the neutral condensations present. To a first order, this approach is validated by models for which we kept $\Pi \times \Delta = 0.25$ constant, since we find that $\langle t^2 \rangle \propto \Delta$, at least when Δ is small (see first 4 models in Table 1). A sequence of models in which we change $\Pi \times \Delta$ is also given in Table 1. Note that since the amplitude of the variations are extreme in the case of an on-off variability type, we expect that $\langle t^2(\text{O}^{+2}) \rangle$ would be substantial as well¹¹. For the

¹¹This is indirectly confirmed by the LINER model of Ercolas, Livio & Binette (1995) who found a significantly higher [O III] $\lambda 4363$ /[O III] $\lambda 5007$ temperature sensitive ratio in their time-dependent model as a result of the very large variability

optimal regime where $\Pi \times \Delta \simeq 1$, a covering factor of 4% is required for the proplyds if we aim to reach $t_{obs.}^2 = 0.025$. Since these models were computed for a low value of \bar{U} , we can estimate that $\langle t^2 \rangle$ would be higher by factor about three, since $\langle t^2 \rangle \propto \sqrt{\bar{U}}$ as discussed in §2.6. Hence maybe a covering factor as low as 1% would suffice. However, the fraction of the Orion nebula volume shadowed by proplyds is estimated to be only 0.1% (William Henney: private communication), which therefore rules out this mechanism.

4. CONCLUSIONS

Our time-dependent models rule out the possibility that the ionizing source variability be the cause of the variations because OB stars are not known to vary at the required 15% level (of Q_H). Furthermore, even if they did, $\langle t^2(\text{O}^{+2}) \rangle$ would still be much smaller than our computed $\langle t^2(\text{H}^+) \rangle$, making the observed values (c.f. Luridiana et al. 1999; Esteban et al. 1998) even more unattainable. As for the model of shadow crossings by opaque condensations, it requires a space density of proplyds a factor ten beyond that estimated by observations.

An interesting and general result about cyclicly variable ionizing sources is that the nebula becomes “on average” less massive but somewhat hotter. Despite the fluctuating size and temperature of the nebula, the *time-averaged* luminosity of all recombination lines remains the same as for the steady-state case. This is also the case for the *time-averaged* energy radiated through all the forbidden lines as compared to the steady-state case (individual forbidden line ratios must in general come out different since the nebula is hotter).

The work of LB was supported by the CONA-CyT grant 32139-E. PF acknowledges support from the Région Rhône-Alpes. The comments received from William Henney about proplyds were particularly useful. We thank Jane Arthur for her contribution during the workshop on 3D-hydro in Mexico City (February 1999) during which the codes YGUANA and YGUAZU were written. We are also indebted to AR who generously funded this event.

A. YGUANA — THE EQUATIONS

In this Appendix, we describe the set of equations used to follow R-type ionization fronts within a spherical nebula photoionized by a variable source. The new code, hereafter called YGUANA, has been

amplitudes of their source.

written in Fortran 77 and will be made accessible to researchers upon request.

We consider the problem of photoionization of a thick spherical gas shell by a central, time-varying source. We make the following simplifying assumptions concerning the source and the gas distribution.

- The ionizing radiation from the central source is taken to be monochromatic at a frequency $\bar{\nu} > \nu_0$ (see value in Table 2) where $h\nu_0 = 13.6$ eV is the ionization potential of hydrogen. The central source is considered point-like (i.e. its characteristic size is much smaller than the inner radius of the gas shell).
- For the purpose of radiation transfer, the gas shell consists only of hydrogen. The gas density is static in time and its value is either a constant or a function of radius.
- The atomic physics is simplified along the lines developed in A.2 and A.3. All essential physical processes are considered (e.g. approximate cooling by metals), although the estimation of their rates is limited to first order approximations.

Given these assumptions, all variables of the problem depend only on the radius from the central source (spherical symmetry) and on the time.

A.1. Time-dependent transfer equation

The time-dependent equation of transfer for monochromatic ionizing radiation, and for spherically symmetric problem is (in spherical coordinates):

$$\frac{1}{c} \frac{\partial \mathcal{F}}{\partial t}(r, t) + \frac{1}{r^2} \frac{\partial (r^2 \mathcal{F})}{\partial r}(r, t) = -\kappa(r, t) \quad (4)$$

where $\mathcal{F}(r, t)$ is the ionizing photon flux (in photon $\text{s}^{-1} \text{cm}^{-2}$) at a radius r from the central source (in cm) and at the time t (in s), $\kappa(r, t)$ is the local opacity at $\bar{\nu}$ (in photon $\text{s}^{-1} \text{cm}^{-3}$), and c is the speed of light (in cm s^{-1}). We have ignored the scattering of the ionizing radiation by dust and the generation of the diffuse field, which would have introduced ‘local’ source terms in equation (4).

For a pure hydrogen medium and monochromatic radiation, the opacity yields the relation:

$$\kappa(r, t) = \bar{\alpha}(\bar{\nu}) \varepsilon n_H(r) [1 - f(r, t)] \mathcal{F}(r, t) \quad (5)$$

where $\bar{\alpha}(\bar{\nu})$ is photoionization cross section of hydrogen at $\bar{\nu}$ (in cm^2), ε is the filling factor of the shell

(assumed uniform and static), $n_H(r)$ is the hydrogen number density (in cm^{-3}), and $f(r, t)$ is the ionization fraction of the hydrogen. The following relation has been used to compute \bar{a} as a function of $\bar{\nu}$:

$$\bar{a}(\bar{\nu}) = 6.3 \times 10^{-18} \left(\frac{\bar{\nu}}{\nu_0} \right)^{-3} \text{ cm}^2 \quad (6)$$

where the value of $\bar{\nu}$ is chosen according to the type of ionizing source and is listed in Table 2. ν_0 is the H ionizing threshold. A monochromatic treatment implies that the progressive hardening of the ionizing radiation (and hence of the temperature) away from the central source cannot be taken into account. Furthermore, in the inner region of planetary nebulae and AGN, heating by photoionization of He^+ is substantial and lead to higher temperatures, this effect cannot be taken into account in our simplified pure hydrogen nebula.

A.2. Time-dependent ionization balance of hydrogen

To solve the transfer equation (4), we need to know the ionization fraction $f(r, t)$ of the hydrogen, and, therefore, to solve the ionization balance of hydrogen. The ionization fraction yields the following equation:

$$\begin{aligned} \frac{\partial f}{\partial t}(r, t) = & \underbrace{\bar{a}(\bar{\nu}) [1 - f(r, t)] \mathcal{F}(r, t)}_{\text{photoionization}} \\ & + \underbrace{\gamma(T) n_H(r) f(r, t) [1 - f(r, t)]}_{\text{collisional ionization}} \\ & - \underbrace{\alpha_B(T) n_H(r) f^2(r, t)}_{\text{recombination}} \end{aligned} \quad (7)$$

where $T(r, t)$ is the temperature of the gas (in K), $\gamma(T)$ is the collisional ionization coefficient (in $\text{s}^{-1} \text{ cm}^3$), and $\alpha_B(T)$ is the recombination rate to excited states of hydrogen (in $\text{s}^{-1} \text{ cm}^3$). We implicitly assume the on-the-spot approximation in our calculations. The following analytical relations have been used to compute γ and α_B as a function of T :

$$\gamma(T) = \exp \left[A + B \times \left(\frac{T}{10^4 \text{ K}} \right)^{-1} \right] \text{ s}^{-1} \text{ cm}^3 \quad (8)$$

with $A = -19$ and $B = -16$, and

$$\alpha_B(T) = 2.6 \times 10^{-13} \left(\frac{T}{10^4 \text{ K}} \right)^{-0.85} \text{ s}^{-1} \text{ cm}^3 \quad (9)$$

A.3. Time-dependent energy balance

The third major equation describing our system is the energy balance equation for the gas:

$$\frac{\partial P}{\partial t}(r, t) = -\frac{2}{3} \Lambda(r, t) \quad (10)$$

TABLE 2
PARAMETERS FOR THE RADIATIVE COOLING CURVE^a AND THE VALUE OF $\bar{\nu}$

Environment	\mathcal{A}	\mathcal{B}	$h\bar{\nu}$ (eV)
H II region	3.8×10^{-24}	4.0×10^{-24}	20 ^b
Planetary nebula	4.0×10^{-24}	3.5×10^{-24}	40 ^c
Active nucleus	4.2×10^{-24}	3.0×10^{-24}	43 ^d

^a \mathcal{A} and \mathcal{B} are in units of $\text{erg s}^{-1} \text{ cm}^3$.

^bStellar atmosphere of temperature 40 000 K.

^cBlack body of temperature 150 000 K.

^dPower law of index -1.3 truncated at 1 keV.

where P is the gas pressure (in dyne cm^{-2}) and Λ is the net cooling rate per unit of volume (in $\text{erg s}^{-1} \text{ cm}^{-3}$). Λ yields the relation:

$$\begin{aligned} \Lambda(r, t) = & + \underbrace{\mathcal{L}(T) n_H^2(r) f^2(r, t)}_{\text{radiative cooling}} \\ & + \underbrace{h\nu_0 \gamma(T) n_H^2(r) f(r, t) [1 - f(r, t)]}_{\text{cooling due to collisional ionization of H}} \\ & + \underbrace{h\nu_0 q(T) n_H^2(r) f(r, t) [1 - f(r, t)]}_{\text{cooling due to collisional excitation of H}} \\ & - \underbrace{\bar{a}(\bar{\nu}) h(\bar{\nu} - \nu_0) n_H(r) [1 - f(r, t)] \mathcal{F}(r, t)}_{\text{heating due to photoionization of H}} \end{aligned} \quad (11)$$

where h is the Planck constant ($6.63 \times 10^{-27} \text{ erg s}$). The coefficients $\mathcal{L}(T)$, $\gamma(T)$, $q(T)$ and $\bar{a}(\bar{\nu})$ are given in Eq. (12), (8), (13) and (6), respectively.

In order to have a realistic energy balance for the gas, the radiative cooling term includes the losses due to metals. $\mathcal{L}(T)$ has been computed using the following relation, which is an analytical fit to the cooling function obtained for a photoionized gas using MAPPINGS 1c and assuming solar metallicities:

$$\mathcal{L}(T) = \mathcal{A} + \mathcal{B} \left(\frac{T}{10^4 \text{ K}} \right)^{2.5} \text{ erg s}^{-1} \text{ cm}^3 \quad (12)$$

where the values of \mathcal{A} , \mathcal{B} depend on the type of environment. Three sets of values are listed in Table 2.

This radiative cooling term applies only to a fully ionized medium. We do not take into account how this term varies with the ionization parameter although we consider separately the cooling due to excitation or ionization of H^0 , which can be significant across ionization fronts. To compute the *net* cooling rate we therefore added to Eq. (11) the cooling terms

due to both collisional ionization and collisional excitation of hydrogen as well as the heating term due to photoionization of hydrogen. The collisional excitation rate $q(T)$ yields the following relation [similar to Eq. (8)]:

$$q(T) = \exp \left[C + D \times \left(\frac{T}{10^4 \text{ K}} \right)^{-1} \right] \text{ s}^{-1} \text{ cm}^3 \quad (13)$$

with $C = -18$ and $D = -11$. The determination of the constants A, B, C and D are based on the coefficients found in Osterbrock (1989).

A.4. Equation of state

In order to close our system of equations, we need to express the equation of state of the gas. We have used the perfect gas equation of state:

$$P(r, t) = [1 + f(r, t)] n_H(r) k T(r, t) \quad (14)$$

where k is the Boltzmann's constant (1.38×10^{-16} erg K $^{-1}$). From Eq. (10) and (14), we can derive the equation for the temperature:

$$\begin{aligned} \frac{\partial T}{\partial t}(r, t) &= \frac{1}{k n_H(r) [1 + f(r, t)]} \\ &\times \left[-\frac{2}{3} \Lambda_{\text{net}}(r, t) - n_H(r) k T(r, t) \frac{\partial f}{\partial t}(r, t) \right] \end{aligned} \quad (15)$$

Together, equations (4), (7) and (15) form a closed system of equations.

B. YGUANA — THE ALGORITHM

In this Appendix, we describe the practical implementation of a code to solve the set of equations describe in A

B.1. Boundary conditions

To solve the problem, we need to define a set of boundary conditions. First, we have to assume initial (i.e. at $t = 0$ s) temperature and ionization structures for the whole shell (i.e. from its inner radius, R_{in} , to its outer radius, R_{out}), as well as the corresponding, initial distribution of ionizing radiation:

$$\forall r, R_{\text{in}} \leq r \leq R_{\text{out}} \quad \begin{cases} f(r, 0) &= f_0(r) \\ T(r, 0) &= T_0(r) \\ \mathcal{F}(r, 0) &= \mathcal{F}_0(r) \end{cases} \quad (16)$$

Last, we need to know the ionizing photon flux of the source $\mathcal{F}_{\text{source}}$ at R_{in} as a function of time:

$$\forall t, \mathcal{F}(R_{\text{in}}, t) = \mathcal{F}_{\text{source}}(t) \quad (17)$$

Assuming that the cavity inside the shell ($r < R_{\text{in}}$) is empty, $\mathcal{F}_{\text{source}}(t)$ can be expressed as a function of the central source ionizing photons production rate, $\mathcal{Q}_{\text{source}}$ (in photon s $^{-1}$):

$$\mathcal{F}_{\text{source}}(t) = \frac{\mathcal{Q}_{\text{source}}(t)}{4\pi R_{\text{in}}^2} \quad (18)$$

B.2. Algorithm

In the following text, the indices i and j refer to the spatial and time axes, respectively.

B.2.1. Transfer equation

Once linearized, equation (4) allows us to compute the ionizing photon flux $\mathcal{F}_{i,j}$ at a radius r_i and time t_j , as a function of the ionization and temperature structures of the shell and of the ionizing photon flux at radii r_{i-1} and r_i , and time t_{j-1} . A sketch of the progression of the computation in the spatial and temporal grids is shown in Fig. 6. We have the following recursive equation for $\mathcal{F}_{i,j}$:

$$\begin{aligned} \mathcal{F}_{i,j} &= \underbrace{\frac{c \delta t}{\delta r} \mathcal{F}_{i-1,j-1} \left(\frac{r_{i-1}}{r_i} \right)^2}_{\text{incoming photon flux (diluted and absorbed)}} \\ &\quad \times \left(1 - \xi_{i-1,j-1} \delta r \frac{r_i^2}{r_{i-1}^2} \right) \\ &\quad + \underbrace{\left(1 - \frac{c \delta t}{\delta r} \right) \mathcal{F}_{i,j-1}}_{\text{out-coming photon flux}} \\ \xi_{i-1,j-1} &= \overline{a}(\overline{\nu}) \varepsilon n_H(r_{i-1}) (1 - f_{i-1,j-1}) \end{aligned} \quad (19)$$

where, $\delta r = r_i - r_{i-1}$, $\delta t = t_j - t_{j-1}$, and c is the speed of light. For this equation to be valid, we must always have:

$$\begin{aligned} c \frac{\delta t}{\delta r} &< 1 \\ \delta r &\ll \left(\frac{r_{i-1}}{r_i} \right)^2 \xi_{i-1,j-1}^{-1} \end{aligned} \quad (20)$$

If δt is larger than the typical atomic physic time scales (e.g. the recombination time), the timestep is divided in smaller time intervals. This prevents $\xi_{i-1,j-1}$ (i.e. the opacity) from changing significantly during the timestep.

B.2.2. Ionization balance

Once $\mathcal{F}_{i,j}$ is computed, the time-dependent ionization balance [equation (7)] is then solved. The new ionization fraction at t_j , $f_{i,j}$, is computed as a function of $f_{i,j-1}$, $T_{i,j-1}$ and $(\mathcal{F}_{i,j} + \mathcal{F}_{i,j-1})/2$. The algorithm used to solve equation (7) is the same as in MAPPINGS 1c (see Appendix in Binette, Dopita & Tuohy 1985).

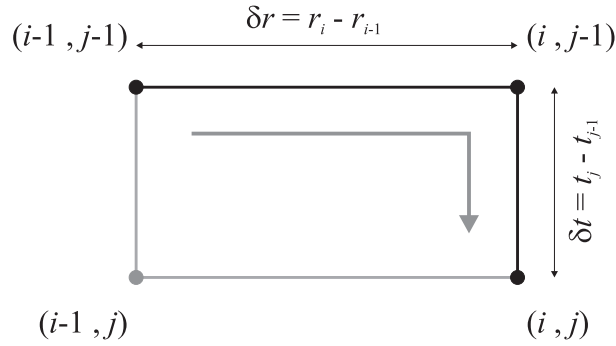


Fig. 6. Sketch of the progression of the computation along the spatial (i index) and temporal (j index) grids.

B.2.3. Temperature equation

At last, the temperature $T_{i,j}$ is computed using the following recursive equation [as derived from Eq. (15)]:

$$\begin{aligned} T_{i,j} &= T_{i,j-1} - \delta t \Theta_{i,j-1} - \Phi_{i,j-1} \\ \Theta_{i,j} &= \frac{2}{3} \frac{\Lambda_{i,j}}{k n_H(r_i) (1+f_{i,j})} \\ \Phi_{i,j} &= \frac{T_{i,j}}{1+f_{i,j}} (f_{i,j+1} - f_{i,j}) \end{aligned} \quad (21)$$

$\Theta_{i,j}$ and $\Phi_{i,j}$ represent the change in temperature due to the net cooling and the change in ‘molecular’ weight, respectively. If necessary, the ionization balance and the temperature equation were solved iteratively.

REFERENCES

- Baldwin, J. A., Ferland, G. J., Martin, P. G., Corbin, M. R., Cota, S. A., Peterson, B. M., & Slettebak, A. 1991, *ApJ* 374, 580
- Binette, L., Dopita, M. A., & Tuohy, I. R. 1985, *ApJ* 297, 476
- Binette, L. & Luridiana, V. 2000, *RevMexAA* 36, 43
- Binette, L., Luridiana, V. & Henney, W. J. 2001, *RevMexAA Conf. Series* 10, 19
- Campbell, A. 1988, *ApJ* 335, 644
- Conti, P. 1972, *ApJ* 174, L79
- Eracleous, M., Livio, M. & Binette, L. 1995, *ApJ* 445, L1
- Esteban, C., Peimbert, Torres-Peimbert, S. & Escalante, V. 1998, *MNRAS* 295, 401
- Ferruit, P., Binette, L., Sutherland, R. S., & Pécontal, E. 1997, *A&A* 322, 73
- Kingdon, J. B. & Ferland, G. J. 1995, *ApJ* 450, 691
- Kingdon, J. B. & Ferland, G. J. 1998, *ApJ* 506, 323
- Liu, X.-W., Storey, P. J., Barlow, M. J., Danziger, I. J., Cohen, M., & Bryce, M. 2000, *MNRAS* 312, 585
- Luridiana, V., Peimbert, M., & Leitherer, C. 1999, *ApJ* 527, 110
- Luridiana, V., Cerviño, M., & Binette, L. 2001, *A&A* 379, 1017

- Osterbrock, D. 1989, in *Astrophysics of gaseous nebulae and active galactic nuclei*, University Science Books: Mill Valley
- Peimbert, M. 1967, *ApJ* 150, 825
- Peimbert, M., Luridiana, V., & Torres-Peimbert, S. 1995, *RevMexAA* 31, 131
- Pérez, E. 1997, *MNRAS* 290, 465
- Stahl, O., Wolf, B., Gäng, T., Gummersbach, C. A., Kaufer, A., Kovacs, J., Mandel, H., & Szeifert, T. 1993, *A&A* 274, L29
- Stasińska, G. & Szczerba, R. 2001, *A&A* 379, 1024
- Torres-Peimbert, S., Peimbert, M., & Peña, M. 1990, *A&A* 233, 540
- van Genderen, A. M., et al. 1989, *A&AS* 79, 263
- Walborn, N. R. 1981, *ApJ* 243, L37

- L. Binette: Instituto de Astronomía, UNAM, Apdo. Postal 70-264, 04510 México, D. F., México (binette@astroscu.unam.mx).
- P. Ferruit: CRAL - Observatoire de Lyon, 9 av. Charles André, F-69561 Saint-Genis-Laval Cedex, France.
- W. Steffen: Instituto de Astronomía, Apdo. Postal 877, 22830 Ensenada, B. C., México.
- A. Raga: Instituto de Ciencias Nucleares, UNAM, Apdo. Postal 70-543, 04510 México, D. F., México.